Journal of the European Ceramic Society **10** (1992) 307–315

Preparation and Properties of Electroconductive Al_2O_3-based Composites

Alida Bellosi, Goffredo De Portu & Stefano Guicciardi*

CNR-IRTEC, Research Institute for Ceramics Technology, Via Granarolo 64, I-48018 Faenza, Italy

(Received 13 January 1992; accepted 28 February 1992)

Abstract

Al_2O_3-based composites with the addition of 20 and 30 vol.% of TiN, TiC, TiB_2 have been produced by hot pressing and by gas-pressure sintering. These electroconductive, toughened and reinforced composites proved to be suitable for the manufacture of complex shapes by electrical discharge machining. Mechanical, electrical and thermal properties have been correlated to the microstructure and to the composition. The mechanical properties of the hot-pressed samples reveal an increase in fracture toughness of 30–70% and in flexural strength of some 70% in comparison with the Al_2O_3 matrix at room temperature. The oxidation, which takes place at the secondary phases, strongly affects the flexural strength at relatively high temperatures ($\approx 700°C$), limiting the potential operating temperature range for this type of composites.

Verbundwerkstoffe auf Al_2O_3-Basis mit 20 und 30 Vol.% TiN-, TiC- oder TiB_2-Zusatz wurden durch Heißpressen und Gasdrucksintern hergestellt. Es wurde gezeigt, daß diese stromleitenden, zähen und verstärkten Verbundwerkstoffe zur Herstellung komplizierter Geometrien durch elektrische Funkenerosion geeignet sind. Die mechanischen Eigenschaften der heißgepreßten Proben zeigen eine Steigerung der Bruchzähigkeit um 30 bis 70% der Biegefestigkeit im Vergleich zur Al_2O_3-Matrix bei Raumtemperatur. Die Oxidation, die zum bevorzugten Angriff sekundärer Phasen führt, beeinflußt deutlich die Biegefestigkeit bei relativ hohen Temperaturen ($\approx 700°C$), wodurch die potentielle Anwendungstemperatur für diese Art von Verbundwerkstoffen begrenzt ist.

Des composites à base d'Al_2O_3 contenant 20 a 30% en volume de TiN, TiC, TiB_2, ont été fabriqués par pressage à chaud et par frittage réaction sous pression. Ces composites renforçés, sont conducteurs électriques; ils ont montré une bonne aptitude à l'usinage par décharge electrique pour la fabrication de formes complexes. Les propriétés mécaniques, électriques et thermiques ont été mises en corrélation avec la microstructure et la composition. On a remarqué que les propriétés mécaniques des échantillons pressés à chaud présentent une résistance mécanique supérieure de 30 a 70% ainsi qu'une résistance à la flexion supérieure de 70% par rapport à une matrice d'Al_2O_3 pressée à température ambiante. L'oxydation, qui a lieu dans la phase secondaire, influence fortement la résistance à la flexion à des temperatures relativement élevées ($\approx 700°C$) ce qui limite l'utilisation de ce type de composite à un certain domaine de températures.

1 Introduction

The development of electroconductive ceramic materials to replace conventional metal parts in special electronic devices will greatly increase the performance of these components as well as the range of applications for ceramics.

In order to obtain such ceramics, an electroconductive phase must be dispersed in the non-conductive ceramic matrix. Hopefully the second-phase reinforcement should allow retention or even an improvement at room and high temperature of the mechanical properties of the matrix without loss of the essential physical property advantages, and this poses limits to the composition of this type of composite. For example, as the dispersed phases have generally less oxidation resistance than the matrix, an excess of their amount must, in any case, be avoided. On the other hand, it is generally known that the maximum toughening effect of the dispersoids is reached between 10 and 30 vol.% of addition,

* To whom correspondence should be addressed.

Journal of the European Ceramic Society 0955-2219/92/$5.00

while for electrical conductivity the minimum amount of dispersoids required ranges from 20 to 30 vol.%, depending on powder particle size and on the chemical composition of the matrix.

Among the potential secondary phases, metallic borides, carbides and nitrides have recently attracted considerable attention. In particular, TiB_2,[1] but also TiN[2] and TiC,[3] have many outstanding properties, such as high melting points, high hardness and electrical conductivity. The addition of these secondary phases to Si_3N_4[4] or SiC[5,6] in amounts higher than 20–30 vol.% were reported to lower drastically the electrical resistivity of the composites down to about 10^{-2}–10^{-5} Ω cm and increase at the same time some mechanical properties, i.e. fracture strength and fracture toughness. Also, in Al_2O_3-based composites with the addition of transition metal nitrides, borides or carbides, good electrical conductivity has been measured.[7–9] These electroconductive toughened ceramics could be shaped by electrical discharge machining[10,11] to manufacture complex components and, at the same time, they can be used as high-temperature heaters, glow-plug heaters and heaters with a controllable specific electrical resistance (i.e. for 12-V automotive batteries, igniters, and so on). Moreover, they could find applications as wear-resistant materials and cutting tools if appropriate second phases are added.

In this study, Al_2O_3-based composites with the addition of 30 vol.% of TiC, TiN, TiB_2 were obtained by hot pressing (hp-samples) and with 20 and 30 vol.% of the same secondary phases by gas-pressure sintering (gps-samples). For these systems thermal expansion, oxidation resistance, electrical and mechanical properties were measured and related to the composition and microstructure.

2 Experimental Procedures

The starting powders were commercial Al_2O_3 (A16-S.G., Alcoa, Bauxite, USA), TiC, TiN and TiB_2 (grades C.a.S., F and C, respectively, H. C. Starck, Berlin) with grain size less than 1·5, 7, 7 and 5 μm, respectively. The particle size distribution of the TiN powder was reduced by the sedimentation technique in order to eliminate the big agglomerates (50–300 μm) present in the as-received batch.

All the mixtures were homogenized in plastic jars with alumina balls and isobutyl alcohol. Samples were hot pressed in a graphite die under vacuum at 1600–1650°C with a pressure of 30 MPa and a heating rate of 30°C/min. Gas-pressure sintering cycles were performed in two steps: at 1800°C and 2 MPa for 60 min and then increasing the pressure up to 9 MPa for 30 min, using N_2 gas for Al_2O_3–TiN and Ar for Al_2O_3–TiC and Al_2O_3–TiB_2.

Microstructural characteristics were studied by X-ray diffraction, scanning electron microscopy (SEM) and microanalysis.

The mean grain size was calculated using the method of intercept of circles on micrographs of thermal etched surfaces. The Young's modulus (E) values were measured on samples with dimensions 8·0 mm × 0·8 mm × 28 mm (width by height by length) by the frequency resonance method.[12] Flexural strength (or Modulus of Rupture) (MOR), both at room and high temperature, was measured on samples 3 mm × 3 mm × 30 mm in a four-point bending fixture, with 26 mm outer span and 13 mm inner span, and a crosshead speed of 0·5 mm/min. In the high-temperature tests, the specimen was held at the set temperature for 10 min before loading to ensure thermal equilibrium. The bars had been previously machined lengthwise with a 100-grit resin-bonded diamond wheel. The last 0·1 mm of thickness was removed at 4 μm/pass. Chamfering of the edges was performed in the same way. The fracture toughness (K_{Ic}) was evaluated by the direct crack measurement (DCM) method with a load of 98 N in a hardness tester (Zwick 3112) using the formula proposed by Anstis *et al.*[13] On the same apparatus the Vickers microhardness ($H_{v0\cdot5}$) was measured on polished surfaces with a load of 4·91 N.

Electrical resistivity (ρ) was measured by the four linear probes method, with a distance among the contact points of 3·78 mm.

The thermal expansion coefficients (α) were measured up to 1000°C, with a heating rate of 5°C/min. Oxidation resistance in air was evaluated on the hp-composites through the continuous weight gain in a TG apparatus during isothermal runs (30 h) at temperatures in the range of 600–1100°C. Electrical discharge machining (EDM) tests were performed on 8-mm-thick hp-samples using brass wire and water as dielectric. This technique was chosen because it is appropriate for very small samples and allows, at the same time, the cleaning and cooling of the surfaces under machining. Removal rate and surface roughness (Ra) were also measured.

3 Results and Discussion

3.1 Densification and microstructure

The shrinkage curves (Fig. 1) and the final densities of the hot-pressed materials (Table 1) point to the

Table 1. Sintering parameters, densities and microstructures of the hot-pressed and gas-pressure sintered composites

Sample	*Sintering parameters*		*Final density*		*Mean grain size*	*Second phase grain size*	*Crystalline phases*
	T (°C)	*t* (*min*)	(*g*/*cm*^{3})	(%)	(μm)	(μm)	
Hot-pressed							
Al_2O_3–30TiN	1650	18	4·39	99·30	0·8	0·1–3·0	Al_2O_3, TiN
Al_2O_3–30TiB_2	1600	18	4·06	98·60	1·3	0·5–7·0	Al_2O_3, TiB_2, 3% $Al_{18}B_4O_{33}$
Al_2O_3–30TiC	1650	18	4·25	98·40	0·9	0·5–3·0	Al_2O_3, TiC
Al_2O_3	1600	10	3·99	100	2·0	—	Al_2O_3
Gas-pressure sintered							
Al_2O_3–20TiN	1800°C, 2 MPa, 60 min + 1800°C, 9 MPa, 60 min		4·27	99·70	3·0	—	Al_2O_3, TiN
Al_2O_3–30TiN			4·38	99·00	2·3		
Al_2O_3–20TiB_2			3·68	90·32	3·5	—	Al_2O_3, TiB_2
Al_2O_3–30TiB_2			3·72	90·45	3·7		
Al_2O_3–20TiC			4·14	99·14	2·1	—	Al_2O_3, TiC
Al_2O_3–30TiC			3·85	90·00	1·6		

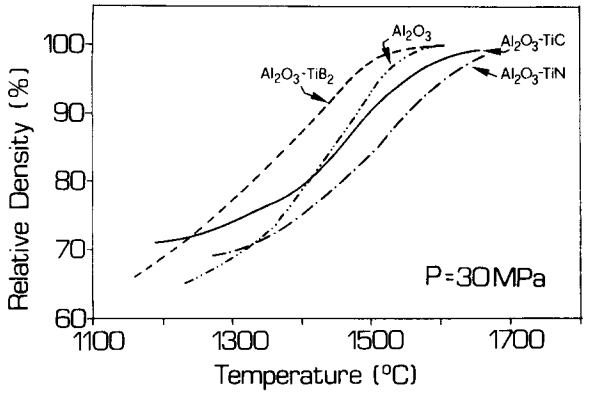

Fig. 1. Densification behaviour under hot-pressing conditions of alumina and alumina-based composites.

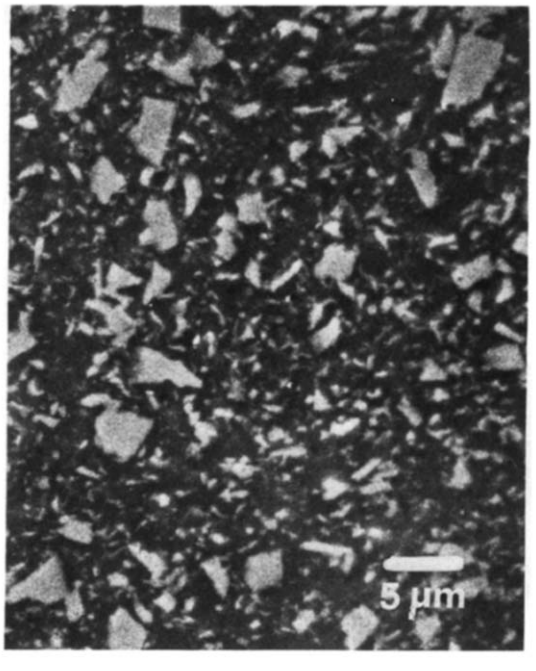

Fig. 2. SEM micrograph of polished surface of the hot-pressed 30 vol.% TiN–Al_2O_3 composite showing a typical microstructure. White areas are TiN particles.

good densification behaviour of all the mixtures. In comparison with the Al_2O_3 matrix, the presence of TiB_2 and TiC lowers the temperature at which densification starts: 1150 and 1180°C, respectively. By contrast, the sample with TiN starts to densify above 1280°C. The presence in the alumina matrix of an inert second phase, such as TiC, TiN or TiB_2, which has limited sinterability, decreases the densification rate by forming an interconnected framework which interferes with the driving forces necessary for bulk diffusion around the inert particles, but its presence seems to have no effect on the ultimate shrinkage. A chemical reaction between the second phase and the matrix was observed only in the sample with TiB_2, with the formation of small amounts of aluminium borate, as the X-ray diffraction analysis indicated. Porosity is virtually absent in the hp-samples containing TiN and TiC, and is very small in the sample with TiB_2. A typical microstructure is shown in Fig. 2 for a 30% TiB_2-composite. Fracture surfaces (Fig. 3(a)–(d)) reveal the different morphologies and grain sizes of the composites in comparison with the hot-pressed Al_2O_3 matrix: the second phase seems to have inhibited the grain growth of Al_2O_3 by slowing down the grain boundary movement.

In the gps-composites an apparent coarsening of the grains occurred for all the systems (Fig. 4(a)–(c) and Table 1), owing to the higher temperatures and the longer holding times with respect to the hot-pressing cycle. This phenomenon is particularly evident in the Al_2O_3–TiB_2 system, in which none of the compositions reached a good density. In this case a high amount of porosity (≈10%) is present and grain size and morphology indicate a microstructural evolution through necking and coalescence. This effect is, of course, linked to the sintering

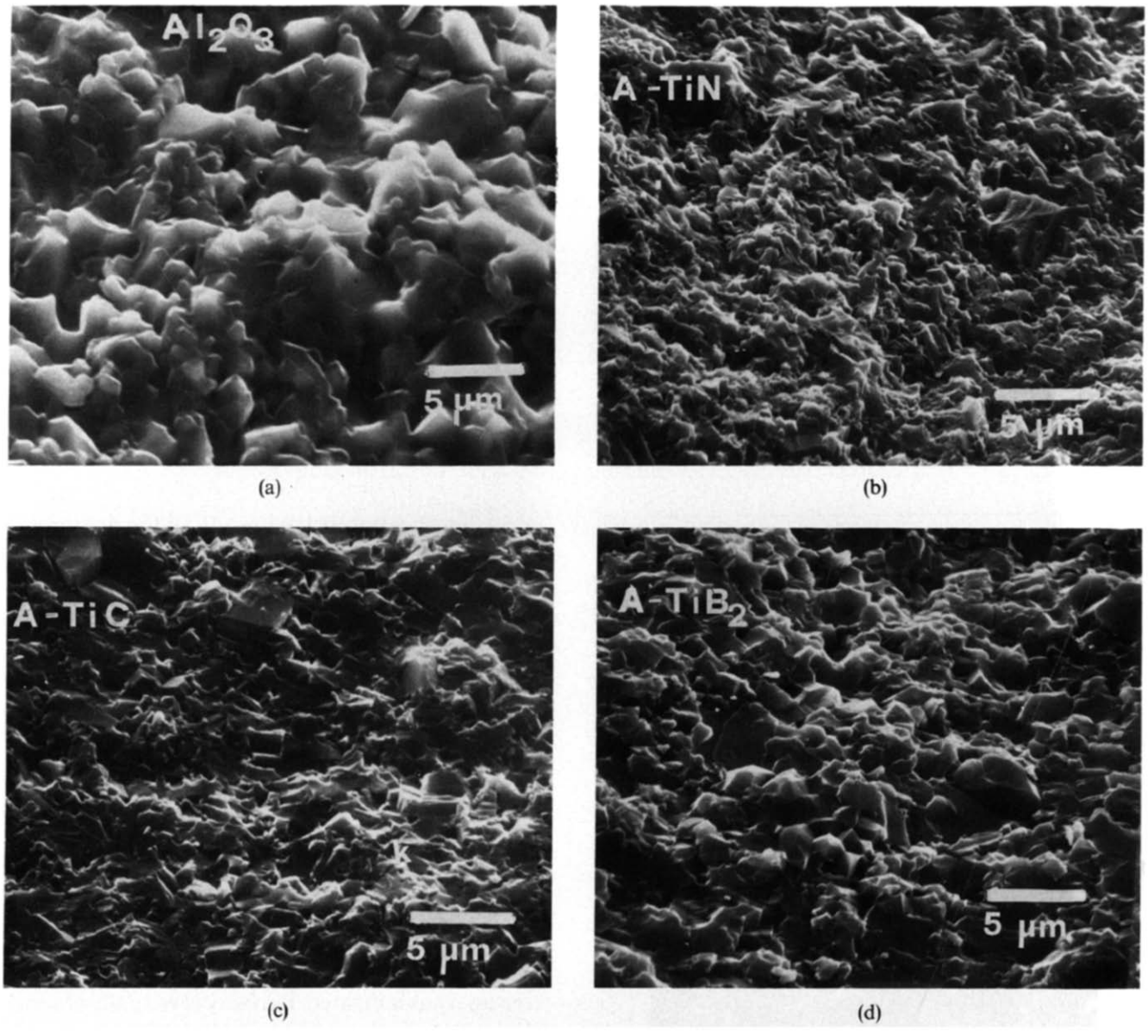

Fig. 3. SEM micrographs of fracture surfaces of the hot-pressed composites: (a) Al_2O_3; (b) 30 vol.% TiN–Al_2O_3; (c) 30 vol.% TiC–Al_2O_3; (d) 30 vol.% TiB_2–Al_2O_3.

Table 2. Thermomechanical and electrical properties of the hot-pressed and gas-pressure sintered composites

Sample	*Electrical resistance, ρ (Ω cm)*	*Thermal expansion (20–1000°C), α × 10⁻⁶ (°C)*	*Young's modulus, E (GPa)*	*Vickers hardness (0·5 kg), $H_{v0·5}$ (GPa)*	*Fracture toughness, K_{Ic} ($MPa\,m^{1/2}$)*	*Four-point bend strength, σ (MPa)*		
						RT	*700°C*	*800°C*
Hot-pressed								
Al_2O_3–30TiN	$6·94 \times 10^{-4}$	8·11	415	19·0 ± 0·6	5·16 ± 0·41	729 ± 53	521 ± 44	448 ± 16
Al_2O_3–30TiB_2	$1·14 \times 10^{-3}$	7·82	424	19·2 ± 0·9	5·65 ± 0·55	711 ± 9	487 ± 23	437 ± 14
Al_2O_3–30TiC	$6·15 \times 10^{-3}$	7·94	410	20·7 ± 0·9	4·27 ± 0·45	785 ± 86	565 ± 52	495 ± 122
Al_2O_3	$>10^{13}$	8·01	396	18·7 ± 0·6	3·24 ± 0·22	436 ± 35	346 ± 35	364 ± 19
Gas-pressure sintered								
Al_2O_3–20TiN	$7·02 \times 10^{-3}$	8·46	411	16·0 ± 0·5	4·35 ± 0·19	510 ± 60	—	—
Al_2O_3–30TiN	$4·74 \times 10^{-4}$		413	16·3 ± 0·4	4·41 ± 0·29	550 ± 57		
Al_2O_3–20TiB_2	—	8·56	297	—	—	215 ± 13	—	—
Al_2O_3–30TiB_2	$7·78 \times 10^{-4}$		341			245 ± 12		
Al_2O_3–20TiC	$5·57 \times 10^{-2}$	8·06	404	18·7 ± 0·4	3·70 ± 0·21	601 ± 38	—	—
Al_2O_3–30TiC	$7·09 \times 10^{-3}$	8·03	313	13·2 ± 0·4	4·12 ± 0·13	368 ± 40		

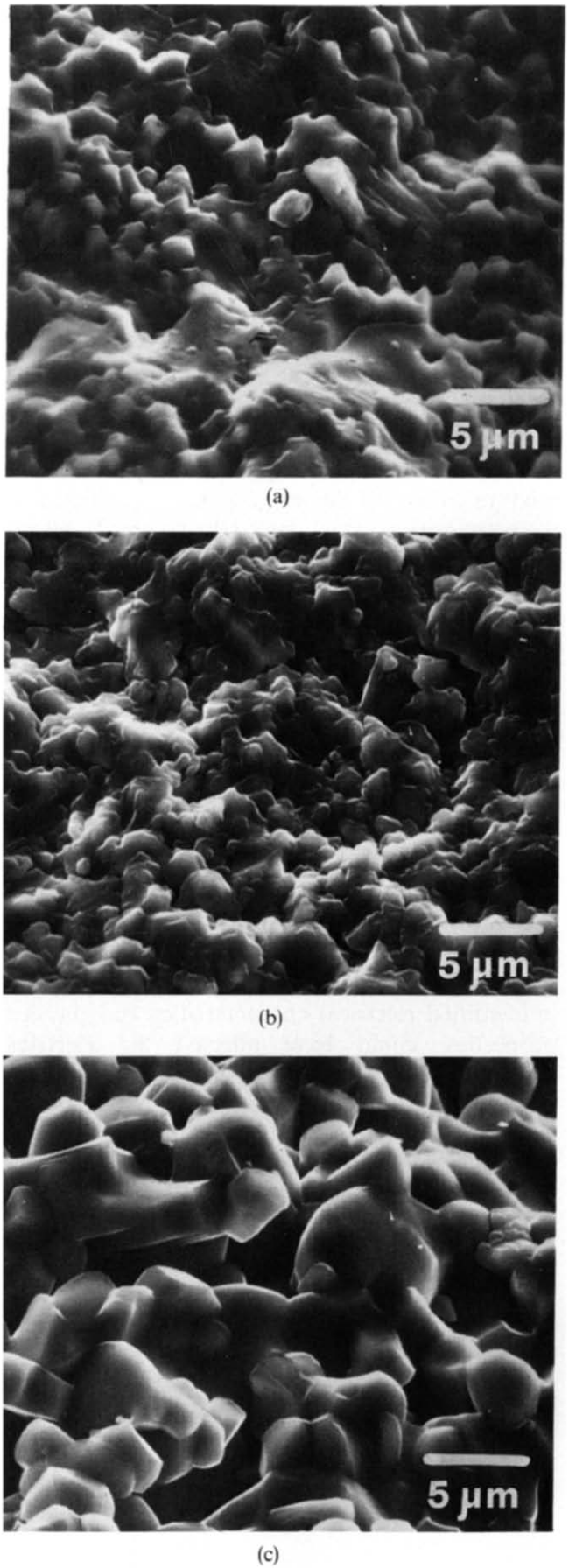

Fig. 4. SEM micrographs of fracture surfaces of the gas-pressure sintered composites: (a) 30 vol.% TiN–Al_2O_3; (b) 30 vol.% TiC–Al_2O_3; (c) 30 vol.% TiB_2–Al_2O_3.

characteristics of TiB_2.[1] The increase in grain size could cause a reduction of the grain boundary area which, in the late sintering stage, impedes the necessary vacancy flux for pore removal. In the Al_2O_3–TiC system, the 20 vol.%-composite was nearly fully dense, while the 30 vol.%-composite was some 10% porous. A second attempt at sintering these two materials gave the same results. It is likely that the complete sintering of the latter material is impeded when too many rigid inclusions (TiC phase) are present. Instead, both the compositions of the Al_2O_3–TiN system were nearly completely dense after the gas-pressure sintering cycle (Table 1).

3.2 Properties

3.2.1 Mechanical properties

Owing to the higher stiffness of all the secondary phases,[14,15] the E values of the composites are higher than that of the matrix and, in the gps-composites, slightly increase as the secondary-phase content increases (Table 2). When a high amount of porosity is present, as in the case of some gps-samples (Table 1), the E values are much lower than those expected. When the densities were comparable, there was almost no difference between the hp-composites and the gps-composites. Using the E values reported in the literature[14,15] for TiN, TiC and TiB_2, it can be seen that the experimental Young's moduli of these composites are close to the lower bound as calculated for particulate composites.[16]

Being harder than the matrix,[14] the introduction of the secondary phases slightly hardens the composites compared to the alumina alone, with the TiB_2-composite having the highest value (Table 2). When the composites were porous, as in the case of some gps-composites, the corresponding hardnesses were greatly reduced. At equal density the hp-samples are harder than the gps-samples by virtue of their finer microstructure. In materials with the same relative density, the increment in the secondary phase from 20 to 30 vol.%, as in the gps-composites, does not induce a significant hardness improvement.

The fracture toughness of all the composites is higher than that of the matrix (Table 2). The hp-composites are generally tougher compared with the gps-composites, with the TiB_2-composite giving the highest value followed by the TiN- and TiC-composite, respectively. Among the gps-composites, in the TiN-reinforced materials there was nearly no difference in fracture toughness between the samples with 20 and 30 vol.% of secondary phase, while in the TiC-reinforced materials the samples with 30 vol.% of secondary phase were tougher, despite their porosity, than the same composite with

20 vol.% of secondary phase, indicating an additional porosity-induced toughening mechanism.[17] For particulate composites, several toughening mechanisms have been proposed: crack pinning,[18] crack deflections,[19] microcracking,[20] crack bridging[21] and residual stresses.[22] A number of these mechanisms can be active at the same time, making it difficult to indicate a prevailing phenomenon. In the present case, since the thermal expansion coefficients of the constituent phases are nearly the same, mechanisms such as residual stresses and microcracking can be excluded. The fracture toughness increment can be attributed more probably to crack deflection and/or crack pinning.

At room temperature the flexural strength of the composites is greatly improved with respect to the matrix when the composites are nearly fully dense (Table 2), and this is a direct consequence of the higher fracture toughness of the composites. In the case of the hp-composite with TiC, moreover, the flexural strength is much higher than that expected from the improvement in fracture toughness, indicating that the secondary phase has also reduced the critical flaw size of the matrix. The flexural strength of the composites reveals the influence of the sintering route followed. In fact the hp-composites are much more resistant than the gps-composites, due to their higher densities and finer microstructure.

In all the systems, the flexural strength of the hp-composites as a function of temperature clearly decreases already at 700°C, with a further diminution at 800°C (Fig. 5). By contrast, the Al_2O_3 matrix, after an initial decrease at 700°C (lower as percentage of the starting value with respect to the composites), remains almost stable at 800°C. In all the materials, the decrease at 700°C is due to the relaxation of residual stresses introduced by machining;[23] in the composites this is also accompanied by the onset of the oxidation that takes place at the secondary phase particles, introducing in this way new surface defects. At 800°C, when the second-phase oxidation is more pronounced, an additional strength reduction occurs in the composites but not in the pure alumina. Nevertheless, at 800°C the flexural strength of the hp-composites is still higher than that of the matrix.

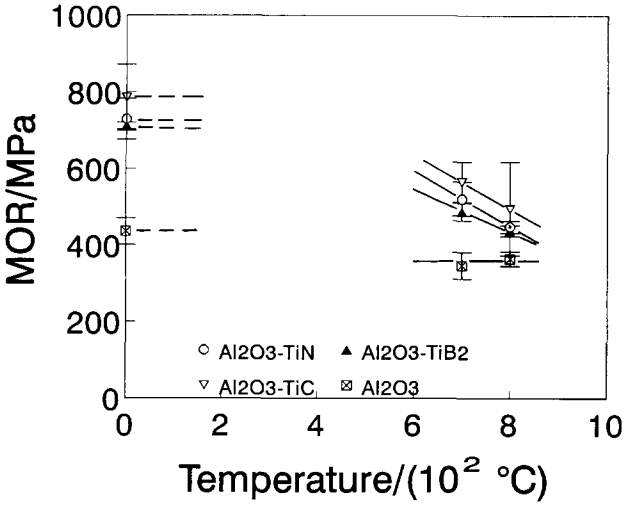

Fig. 5. Modulus of Rupture (MOR) or flexural strength as a function of temperature in the hot-pressed composites. Symbols and bars represent mean values and standard deviations, respectively.

3.2.2 *Thermal and electrical properties*

The thermal expansion coefficients of the composites (Table 2) follow approximately the rule of mixture where the thermal expansion coefficient of the composite, α_c, is related to the volume fractions, V_1 and V_2, and thermal expansion coefficients, α_1 and α_2, of each phase according to

$$\alpha_c = \alpha_1 V_1 + \alpha_2 V_2 \quad (1)$$

The dilatometric curves have no hysteresis, suggesting the absence of microcracks in the sintered body.

The values of the electrical resistivity reveal a slight difference in the three types of composites (Fig. 6 and Table 2). Considering that the resistivity of the second phases (Table 1) is about the same,[1-3] the lower resistivity of Al_2O_3–TiN could be associated with the finer particle size of TiN,[4,24] in comparison with TiC and TiB_2. Moreover, in the hp-composites with TiB_2, the presence of aluminium borate, with unidentified electrical characteristics and physical properties, could have affected the electrical behaviour. The gps-samples show a slightly lower resistivity in most of the cases with respect to the hp-composites. The resistivity measurements on the 20 vol.% composites with TiN and TiC show that the percolation threshold for conductivity has been

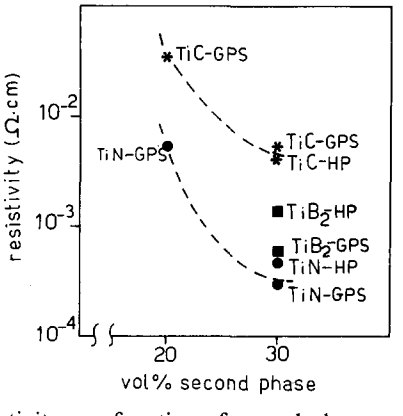

Fig. 6. Resistivity as a function of second-phase content in the hot-pressed and gas-pressure sintered composites.

reached already at this level of second-phase content.

3.3 Oxidation resistance

As TiN, TiC, TiB_2 are easy-to-oxidize phases, their use as secondary phases strongly affects the thermal stability of the composites.

The weight gain as a function of the temperature after 1000 min of isothermal oxidation is shown in Fig. 7.

Al_2O_3–TiN and Al_2O_3–TiB_2 samples start to oxidize at about 700°C, while Al_2O_3–TiC samples start at about 800°C. Afterwards, two distinct behaviours are observed: the oxidation of Al_2O_3–TiC and Al_2O_3–TiN considerably increases with the increase in temperature, whereas Al_2O_3–TiB_2, after a high oxidation at about 800°C, shows a progressive stability up to 1100°C.

The behaviour can be explained on the basis of the structure and composition of the oxide scale and of the kinetics of the process, which are reported elsewhere.[25] Briefly, in the cases of Al_2O_3–TiC and Al_2O_3–TiN, at $T > 800$°C the oxidation shows a first stage (up to 600 min) which is governed by diffusion-controlled kinetics. For a longer time, the oxidation behaviour is approximately linear and the oxide layer (Fig. 8(a) and (b)) shows the formation of a TiO_2 scale which is probably non-protective, owing to the formation of cracks that increase the active area for oxidation.

In the case of the Al_2O_3–TiB_2 at $T > 800$°C, the oxide scale (Fig. 8(c)) is mainly composed of crystalline phases of $Al_4B_2O_9$, in addition to TiO_2, which could help to protect the bulk from the massive oxidation of TiB_2 particles.

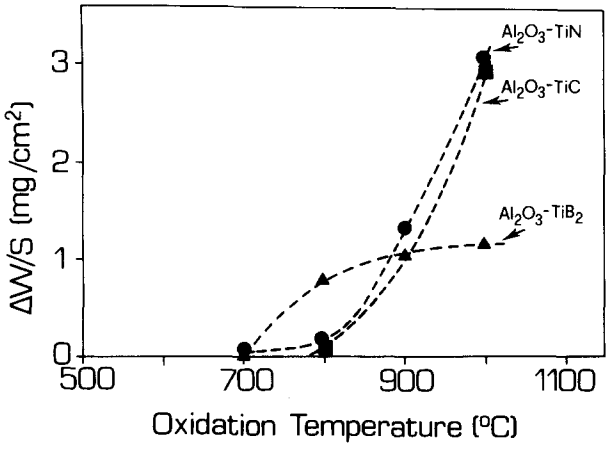

Fig. 7. Specific oxidation weight gain, $\Delta W/S$, of the hot-pressed composites as a function of the oxidation temperature (oxidation time 1000 min). The specific oxidation weight gain is obtained by dividing the total weight gain, ΔW, of the sample by the surface, S, exposed to the oxidizing atmosphere.

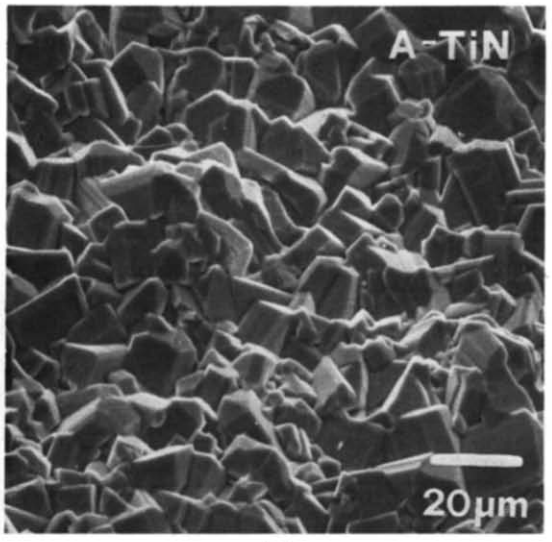

(a)

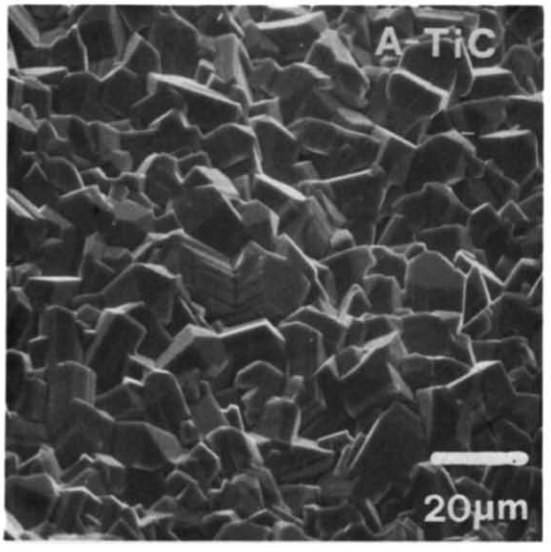

(b)

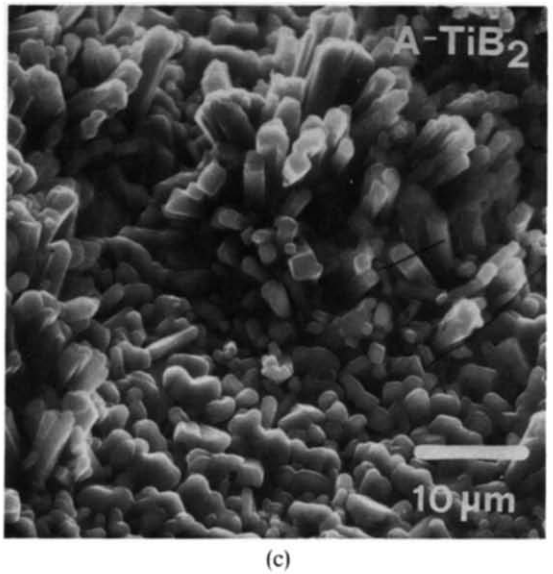

(c)

Fig. 8. SEM micrographs of the oxidized surfaces ($T = 1000$°C) of the hot-pressed composites: (a) 30 vol.% TiN–Al_2O_3; (b) 30 vol.% TiC–Al_2O_3; (c) 30 vol.% TiB_2–Al_2O_3.

3.4 Electrical discharge machining (EDM)

For all the composites the electrical conductivity level was good enough for EDM. The material removal rate measured during the machining and the roughness of the as-cut surfaces (Fig. 9) suggests an easier machinability of the composites containing TiB_2 and TiN; for the sample with TiC the material removal rate is two and four times lower than that for Al_2O_3–TiB_2 and Al_2O_3–TiN, respectively. Both material removal rate and surface roughness (therefore the damaged layer thickness) seem to be directly related to the electrical resistivity of the samples: the higher the resistivity, the higher the surface roughness and the lower the cutting rate.

Figure 10(a)–(c) compare the microstructure of the machined surfaces. Discharges create craters and the overall surface appears pitted with rounded molten-looking bumps with overlapping craters of varying diameter and morphology. The damage and crater size increase with the decrease in cutting speed. Al_2O_3–TiC samples show significant surface damage with microcracking and small droplets (white areas in Fig. 10(b)) which are resolidified brass from wire as resulted from micro-analysis.

X-Ray diffraction analyses of the machined surfaces show no oxidation of the second phase. Besides the starting phases, brass is present in the Al_2O_3–TiC samples and, in lesser amount, in the Al_2O_3–TiB_2 samples. The morphological and structural characteristics of the machined surfaces are directly related to the material removal mechanisms which depend on the interactions between the characteristics of the phases constituting the material and the parameters adopted during EDM. Generally, for machining hard and brittle ceramics,

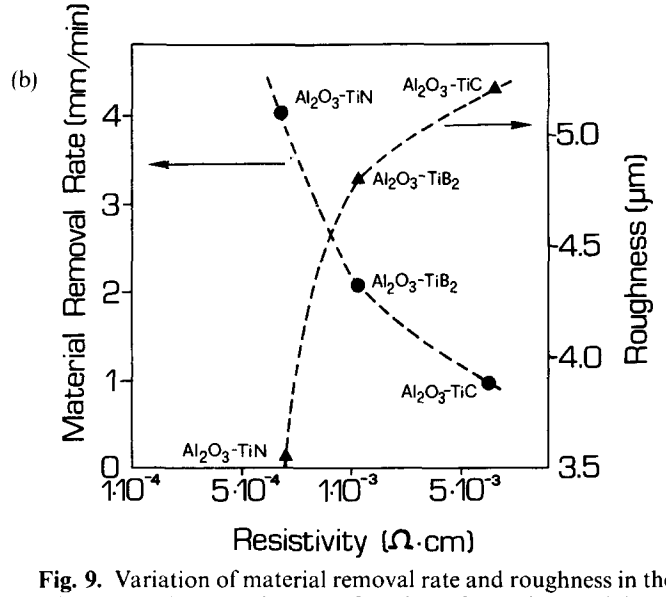

Fig. 9. Variation of material removal rate and roughness in the hot-pressed composites as a function of sample resistivity.

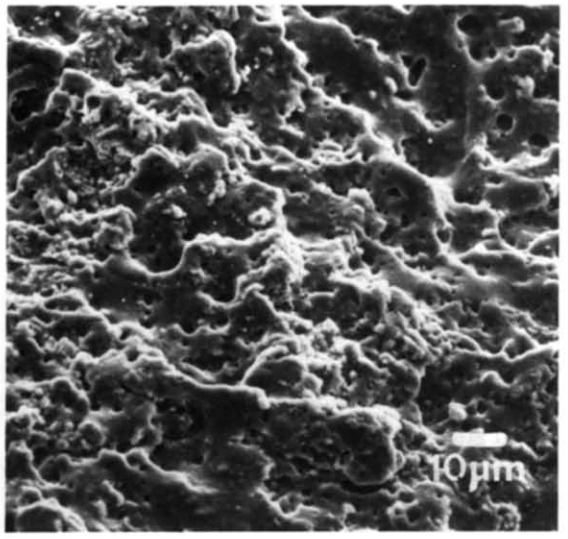

(a)

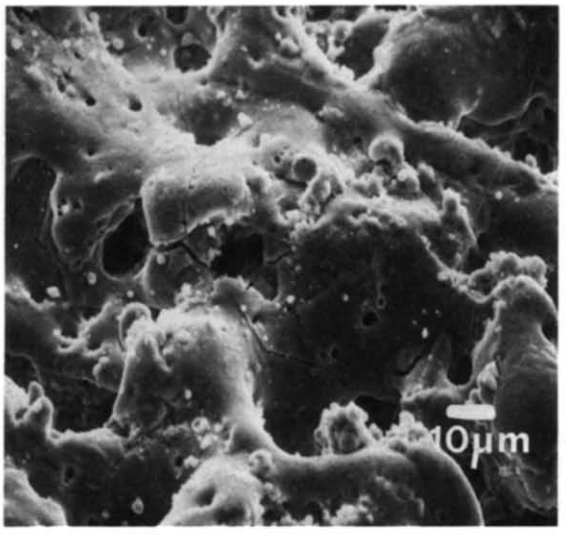

(b)

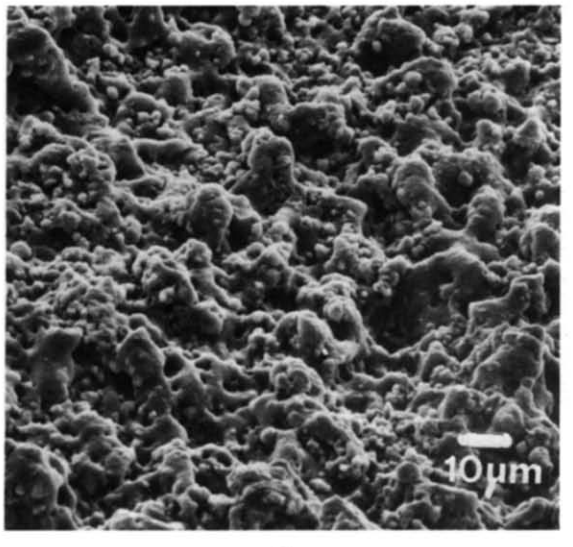

(c)

Fig. 10. SEM micrographs of surfaces of hot-pressed composites after EDM: (a) 30 vol.% TiN–Al_2O_3; (b) 30 vol.% TiC–Al_2O_3; (c) 30 vol.% TiB_2–Al_2O_3. Note the extensive cracking in (b).

EDM takes place by melting, evaporating or fracturing the surface.[11] In the present case it is reasonable to assume from the morphological characteristics that the surface was mainly formed by resolidified molten material. The amount of material that solidifies and adheres to the surface is a function of the composition. In the surface scale, the secondary phases are present in a higher amount with respect to the Al_2O_3 than in the bulk.

4 Conclusions

High-strength Al_2O_3-based composites with low electrical resistivity were manufactured with 20 and 30 vol.% additions of TiN, TiC and TiB_2 particles by hot-pressing and gas-pressure sintering.

Apart from the conductivity itself, the most attractive properties of this new class of electroconductive particulate-reinforced ceramics are improved fracture toughness and strength, and the possibility of using electrical discharge machining (EDM) instead of conventional techniques to make components of complex shape.

The hot-pressed composites were found to be better than the gas-pressure sintered composites in terms of mechanical properties, owing to their higher density and finer microstructure. On the other hand, the gas-pressure sintered composites gave higher conductivity values.

EDM machinability, i.e. rate and final roughness, has been shown to be largely dependent on the type of electroconductive phase employed.

Oxidation rates and high-temperature flexure tests indicate that the most crucial feature of this type of composites is the very low oxidation resistance.

References

1. Bellosi, A., Graziani, T., Guicciardi, S. & Tampieri, A., Characteristics of TiB_2 ceramics. In *Proc. Special Ceramics 9*, London, 18–20 December 1990. Institute of Ceramics, Shelton, Stoke-on-Trent, Staffs, UK.
2. Engineering property data on selected ceramics, Vol. 1: Nitrides. MCIC report, ed. Metals and Ceramics Information Center, Battelle, Columbus, Ohio, 1976, 5.3.4-1–5.3.4-9.
3. Engineering property data on selected ceramics, Vol. 2: Carbides. MCIC report, ed. Metals and Ceramics Information Center, Battelle, Columbus, Ohio, 1987, 5.2.3-1–5.2.3-26.
4. Bellosi, A., Guicciardi, S. & Tampieri, A., Development and characterization of electroconductive Si_3N_4–TiN composites. *J. Eur. Ceram. Soc.*, **9** (1992) 83–93.
5. McMurtry, C. H., Boecker, W. D. G., Seshadri, S., Zanghi, J. S. & Garnier, J. E., Microstructure and material properties of SiC–TiB_2 particulate composites. *Am. Ceram. Soc. Bull.*, **60** (1987) 325–9.
6. Endo, H., Ueki, M. & Kubo, H., Microstructure and mechanical properties of hot-pressed SiC–TiC composites. *J. Mat. Sci.*, **26** (1991) 3769–74.
7. Kimura, I., Hotta, N., Hiraoka, Y., Saito, N. & Yokota, Y., Sintering and characterization of Al_2O_3–TiB_2 composites. *J. Eur. Ceram. Soc.*, **5** (1989) 23–7.
8. Matsushima, J., Shinsuke, H. & Saito, H., Pressureless sintering of TiB_2–Al_2O_3. *J. Ceram. Soc. Jpn (Int. Ed.)*, **97** (1989) 1200–5.
9. Ishigaki, T., Sato, K. & Moriyoshi, Y., Pressureless sintering of TiC–Al_2O_3 composites. *J. Mat. Sci.*, **8** (1989) 678–80.
10. Ramulu, M., EDM sinker cutting of ceramic particulate composite, SiC–TiB_2. *Adv. Ceram. Mat.*, **3** (1988) 324–7.
11. Petrotes, N. F. & Gadalla, A. M., Electrical discharge machining of advanced ceramics. *Am. Ceram. Soc. Bull.*, **67** (1988) 1048–52.
12. ASTM C848-78 (Reapproved 1983), Standard test method for Young's modulus and Poisson's ratio for ceramic whitewares by resonance.
13. Anstis, G. R., Chantikul, P., Lawn, B. R. & Marshall, D. B., A critical evaluation of indentation technique for measuring fracture toughness: I. Direct crack measurements. *J. Am. Ceram. Soc.*, **64** (1981) 533–8.
14. *Ceramic Source '90*, Am. Ceram. Soc., 5, 1989, p. 315.
15. Desmaison-Brut, M., Glandus, J. C., Montintin, J., Valin, F. & Boncour, M., Elastic moduli–porosity relations in transition metal nitrides: TiN, ZrN, HfN and TaN. In *Ceramics Today—Tomorrow's Ceramics, Material Science Monographs*, 66, ed. P. Vincenzini. Elsevier Science Publishers, Amsterdam, 1991, pp. 1713–20.
16. Ashby, M. F. & Jones, D. R. H., *Engineering Materials*. Pergamon Press, Oxford, 1980, pp. 59–61.
17. Rice, W. R., Ceramic matrix composite toughening mechanisms: an update. *Ceram. Eng. Sci. Proc.*, **6** (1985) 589–607.
18. Green, D. J., Fracture toughness predictions for crack bowing in brittle particulate composites. *J. Am. Ceram. Soc.*, **66** (1983) C4–C5.
19. Faber, K. T. & Evans, A. G., Crack deflection processes—I. Theory. *Acta Metall.*, **31** (1983) 565–76.
20. Evans, A. G. & Faber, K. T., Toughening of ceramics by circumferential microcracking. *J. Am. Ceram. Soc.*, **64** (1981) 394–8.
21. Budiansky, B., Amazigo, J. C. & Evans, A. G., Small-scale crack bridging and the fracture toughness of particulate-reinforced ceramics. *J. Mech. Phys. Solids*, **36** (1988) 167–87.
22. Taya, M., Hayashi, S., Kobayashi, A. S. & Yoon, H. S., Toughening of a particulate-reinforced ceramic-matrix composite by thermal residual stress. *J. Am. Ceram. Soc.*, **73** (1990) 1382–91.
23. Johnson-Walls, D., Evans, A. G., Marshall, D. B. & James, M. R., Residual stresses in machined ceramic surfaces. *J. Am. Ceram. Soc.*, **69** (1986) 44–7.
24. Martin, C., Cales, B., Vivier, P. & Mathieu, P., Electrical discharge machinable ceramics composites. *Mat. Sci. Eng.*, **A109** (1989) 351–6.
25. Tampieri, A., Biasini, V. & Bellosi, A., Oxidation of monolithic TiB_2 and of Al_2O_3–TiB_2 composites. In *The Proceedings of the Second European Ceramic Society Conference*, Augsburg, FRG, 11–14 September 1991.